Solar Aluminum Production by Vacuum Carbothermal Reduction of Alumina—Thermodynamic and Experimental Analyses

M. KRUESI, M.E. GALVEZ, M. HALMANN, and A. STEINFELD

Thermochemical equilibrium calculations indicate the possibility of significantly lowering the onset temperature of aluminum vapor formation *via* carbothermal reduction of Al_2O_3 by decreasing the total pressure, enabling its vacuum distillation while bypassing the formation of undesired by-products Al_2O, Al_4C_3, and Al-oxycarbides. Furthermore, the use of concentrated solar energy as the source of high-temperature process heat offers considerable energy savings and reduced concomitant CO_2 emissions. When the reducing agent is derived from a biomass source, the solar-driven carbothermal reduction is CO_2 neutral. Exploratory experimental runs using a solar reactor were carried out at temperatures in the range 1300 K to 2000 K (1027 °C to 1727 °C) and with total pressures in the range 3.5 to 12 millibar, with reactants Al_2O_3 and biocharcoal directly exposed to simulated high-flux solar irradiation, yielding up to 19 pct Al by the condensation of product gases, accompanied by the formation of Al_4C_3 and Al_4O_4C within the crucible. Based on the measured CO generation, integrated over the duration of the experimental run, the reaction extent reached 55 pct at 2000 K (1727 °C).

DOI: 10.1007/s11663-010-9461-6

I. INTRODUCTION

THE production of aluminum *via* the Hall–Héroult electrolytic process is characterized by its high-energy consumption (approximately 45 GJ/ton Al) and its associated high-specific greenhouse gas emissions (4.9 to 7.4 ton CO_{2equiv}/ton Al).[1–3] The alternative path *via* carbothermal reduction of Al_2O_3 can be represented by the following overall reaction:

$$Al_2O_3 + 3C = 2Al + 3CO \quad [1]$$

However, reaction [1] is complicated by the formation of undesired by-products such as aluminum carbide Al_4C_3, oxycarbides Al_2OC and Al_4O_4C, and the lower valence oxide Al_2O.[4,5] One approach to overcome this difficulty was to reduce the Al_2O-Al-CO gas mixture by carbon at about 2273 K (2000 °C).[6] According to the Le Chatelier principle, the extent of the chemical reaction should be favored by a decrease in the total gas pressure. Thus, under vacuum conditions, the equilibrium of reaction [1] should be shifted to the right and the onset temperature for the metal production should be lowered significantly. This principle had been applied successfully in the production of magnesium and silicon. The carbothermal reduction of MgO in calcined dolomite yielded Mg using a moderate vacuum of 1.33 millibar at 1673 K (1400 °C).[7] The silicothermic reduction of CaO-MgO in the industrial Pidgeon process for magnesium was achieved by reacting CaO-MgO with ferrosilicon in evacuated retorts at 1450 K to 1800 K (1177 °C to 1527 °C) and less than 1.33×10^{-4} bar.[8–10] The production of Si by vacuum carbothermal reduction of SiO_2 in the range 1997 K to 2263 K (1724 °C to 1990 °C) at ~3×10^{-5} bar yielded Si/SiO_2 mixtures condensed from the gas phase, with 79 wt pct Si content.[11]

As will be shown in the following analysis, reaction [1] is highly endothermic ($\Delta H_{298\ K} = 1344$ kJ/mol) and proceeds at higher than approximately 1500 K (1227 °C) when operating at 10^{-4} bar. The use of concentrated solar energy as the source of high-temperature process heat significantly reduces the discharge of greenhouse gases and other pollutants derived from the combustion of fossil fuels.[12,13] Previous relevant metallurgical processes performed in solar furnaces include the carbothermal and methanothermal reductions of Fe_3O_4, MgO, ZnO, and SiO_2 to produce Fe, Mg, Zn, and Si, respectively[11,14–17]; the carbothermal reductions of Al_2O_3, CaO, SiO_2, and TiO_2 in an Ar flow to produce Al_4C_3, CaC_2, SiC, and TiC, respectively[17]; and the carbothermal reductions of Al_2O_3, SiO_2, TiO_2, and ZrO_2 in a N_2 flow to produce AlN, Si_3N_4, TiN, and ZrN, respectively.[17–19] The present study thermodynamically examines the vacuum carbothermal reduction of Al_2O_3 and demonstrates experimentally the production of Al using a biomass-based reducing agent and simulated concentrated solar energy.

M. KRUESI, Doctoral Student, is with the Department of Mechanical and Process Engineering, ETH Zurich, 8092 Zurich, Switzerland. M.E. GALVEZ, Scientist, is with the Instituto de Carboquimica, Miguel Luesma Castan, 50018 Zaragoza, Spain. M. HALMANN, Professor, is with the Department of Environmental Sciences and Energy Research, Weizmann Institute of Science, Rehovot 76100, Israel. A. STEINFELD, Professor, is with the Department of Mechanical and Process Engineering, ETH Zurich, and with the Solar Technology Laboratory, Paul Scherrer Institute, 5232 Villigen, Switzerland. Contact e-mail: aldo.steinfeld@ethz.ch
Manuscript submitted May 6, 2010.
Article published online December 14, 2010.

II. THERMODYNAMIC ANALYSIS

Thermochemical equilibrium computations were carried out using the FactSage code.[20] Reaction enthalphies were calculated using NIST webbook data[21] and HSC Outokumpu code.[22] The equilibrium compositions as a function of temperature for the system $Al_2O_3 + 3C$ at 1, 10^{-5}, and 10^{-6} bar are shown in Figures 1 through 3. As observed in Figure 1, at atmospheric pressure, the production of elementary Al(g), essentially free of Al_2O and Al_4C_3, is thermodynamically favorable above 2800 K (2527 °C) (*i.e.*, at a practically prohibitive high temperature). Figures 2 and 3 show that lowering the gas pressure to 10^{-5} or 10^{-6} bar not only shifts the formation of Al(g) to much lower temperatures but it also frees the Al(g) production from the undesired by-products Al_2O and Al_4C_3 already at more accessible temperatures. The temperatures for the onset of Al formation at approximately 0.001 pct conversion of Al_2O_3 to Al for gas pressures of 10^{-6} to 1 bar are listed in Table I. At 1800 K (1527 °C) and 10^{-4} bar, the system in equilibrium mainly consists of a gas mixture containing 40 pct Al(g) to 60 pct CO(g), with small traces of Al_2O(g).

In a preliminary environmental evaluation of the potential of such a vacuum thermochemical process, it is assumed that either concentrated solar radiation or coal combustion is applied as the energy source of process heat. Furthermore, it is proposed that the CO released would be water–gas shifted to syngas followed by methanol synthesis, as shown in Table II. The total enthalpy change of the reaction was calculated in the following steps: (1) for the stoichiometric reaction $Al_2O_3(s) + 3C(gr) = 2Al(g) + 3CO(g)$ at 1 bar and 1800 K (1527 °C), ΔH = 1941.1 kJ/mol Al_2O_3; (2) for the theoretical work of isothermal expansion of the product gases at 1800 K (1527 °C) from 1 to 10^{-4} bar, $\Delta G = nRTlnp$ = 698 kJ/mol Al_2O_3. Thus, the total theoretical heat and work input would amount to 49 GJ/ton Al and is comparable with that in the Hall–Héroult electrolytic process. In case the reducing agent is derived from a biomass source, the solar-driven carbothermal reduction would be CO_2-neutral. The exergy efficiency, defined by the ratio of maximal work output that can be extracted from the products—given by the Gibbs free energy change of the complete combustion of the products 2Al + 3CO and assuming 90 pct chemical yield—to the sum of the reaction process heat (*i.e.*, net solar energy input), the high heating value of the reactants, and the pump work to the required vacuum, all calculated at 298 K (25 °C), would be 61 pct.

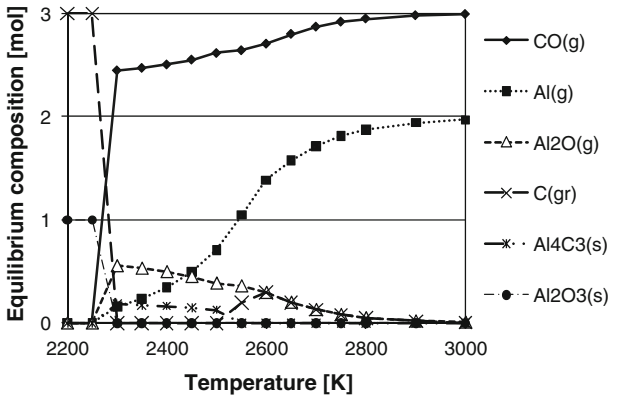

Fig. 1—Variation of the equilibrium composition as a function of temperature for the system $Al_2O_3 + 3C$ at 1 bar.

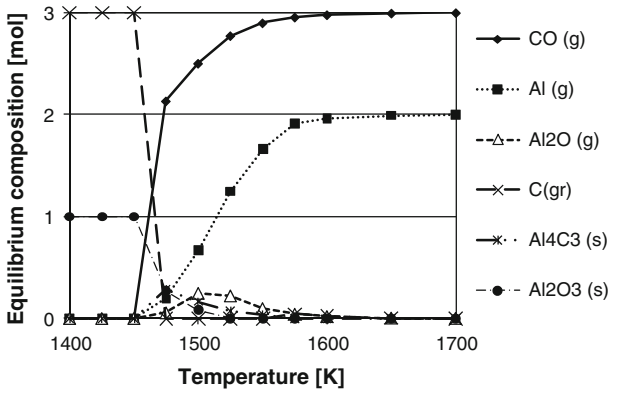

Fig. 2—Variation of the equilibrium composition as a function of temperature for the system $Al_2O_3 + 3C$ at 10^{-5} bar.

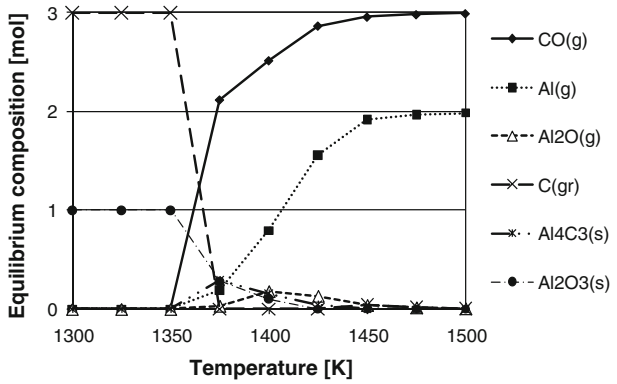

Fig. 3—Variation of the equilibrium composition as a function of temperature for the system $Al_2O_3 + 3C$ at 10^{-6} bar.

Table I. Equilibrium Temperatures for the Onset of Al Formation at 10^{-5} Mole Fraction for the System $Al_2O_3 + 3C$

Pressure (Bar)	Temperature
10^{-6}	1370 K (1097 °C)
10^{-5}	1465 K (1192 °C)
10^{-4}	1580 K (1307 °C)
0.001	1703 K (1430 °C)
0.01	1855 K (1582 °C)
0.1	2037 K (1764 °C)
0.5	2190 K (1917 °C)
1.0	2258 K (1985 °C)

Table II. Preliminary Evaluation of the Annual Coproduction Al and CH_3OH by Vacuum Carbothermic Reduction of Al_2O_3 from a Mixture of Al_2O_3 and Coke, Initially at 300 K (27 °C) and 1 Bar, Transformed at 1800 K (1527 °C) and 10^{-4} Bar According to Eq. [1]. Process Heat Supplied Either by Concentrated Solar Energy or by Coal Combustion

Design Al_2O_3 feed (kmol/yr)	1.00×10^6
Annual process heat (GJ/yr)	1.96×10^6
Annual coke feed (ton/yr)	1.18×10^6
Annual coal feed (ton/yr)*	0.048×10^6
Annual pumping energy (GJ/yr)†	0.84×10^6
Total annual fuel input (GJ/yr)‡	2.02×10^6
Total annual fuel input (GJ/yr)*	3.98×10^6
Annual Al production (ton/yr)ξ	0.040×10^6
Annual methanol production (ton/yr)¶	0.0288×10^6
Total annual CO_2 release (ton/yr)‡	0.088×10^6
Total annual CO_2 release (ton/yr)*	0.26×10^6

*Assuming coal combustion for process heat.
†Assuming 50 pct efficiency in electricity production.
‡Assuming solar energy for process heat; Ton = metric ton.
ξAssuming 75 pct overall yield in production of Al.
¶Assuming 90 pct overall yield in the water–gas shift of 2/3 of CO to syngas, converted to methanol.

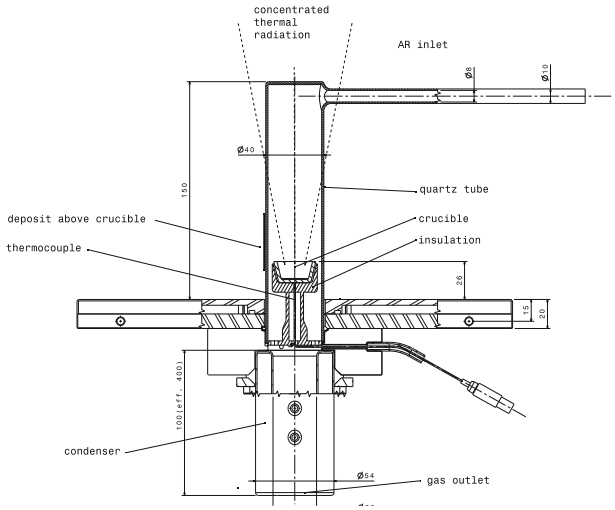

Fig. 4—Scheme of the vacuum solar reactor featuring a quartz tube containing a glassy carbon crucible with reactants directly exposed to concentrated solar radiation.

III. EXPERIMENTAL ANALYSIS

Exploratory experimental runs were carried out at the High-Flux Solar Simulator (HFSS) of the Paul Scherrer Institute.[23] This research platform consists of an array of high-pressure Xe arcs, each close-coupled to elliptical specular reflectors capable of delivering 50 kW of continuous radiative power, mostly in the visible and infrared (IR) spectra, with peak flux intensities equivalent to solar concentration ratios of up to 11,000 suns (1 sun = 1 kW/m^2). Thus, the solar reactor is tested under comparable heat-transfer characteristics of highly concentrated solar systems, such as solar dishes and solar towers, and can reach temperatures exceeding 2000 K (1727 °C) at heating rates exceeding 1000 K/s. Power flux intensities are adjustable by the number of Xe arcs in operation, the position of the venetian shutter, and the position of the test target relative to the focal plane.

The vacuum solar reactor is shown schematically in Figure 4. It consists of a vertical transparent quartz tube (length 150 mm, diameter 40 mm, and wall thickness 2 mm) containing a glassy carbon crucible (Sigradur G, HTW Hochtemperatur-Werkstoffe GmbH, Thierhaupten, Germany; diameter 29 mm, height 15 mm, and thickness 2 mm), supported by an insulating ZrO_2/Al_2O_3 holder with a type-S thermocouple touching the bottom of the crucible. The reactor is positioned facing up, whereas a 45 deg mirror is implemented to redirect down the HFSS beam. With this arrangement, the reactants are directly exposed to concentrated thermal radiation, providing an efficient mean of heat transfer directly to the reaction site. The quartz tube is closed at the top and has a side inlet for Ar flow, which serves as a carrier for emerging gaseous species. The outlet at the bottom of the quartz tube is connected to a water-cooled steel plate with Viton sealing O-rings protected by an Al_2O_3 radiation shield followed by a water-cooled condenser, a paper filter (Whatman, Kent, UK; Grade GF/A, 1.6 μm), and a vacuum pump (Alcatel, Annecy, France; 20012A, dual stage, rotary vane, maximal flow 12 m^3/h).

The Ar mass flow rate was kept at 1 l/min (normal conditions) using an electronic flowmeter (Bronkhorst HI-TEC, Ruurlo, The Netherlands). Pressure was measured with a vacuum differential pressure sensor (SMC, Tokyo, Japan; PSE-540). Product gas composition was monitored online by an IR gas analyzer (Ultramat 23, Siemens, Munich, Germany; 0.2 pct detection limit, 1-Hz sampling rate). The composition of solid products was determined by X-ray powder diffraction (XRD, Philips, Amsterdam, The Netherlands; XPert MPD/DY636, CuK_α, $\lambda = 1.540598$ Å, $2\theta = 20$ to 80 deg, step size 0.05 deg). Solid samples were characterized by means of their particle size distribution measured by laser scattering (LA-950 analyzer; HORIBA, Kyoto City, Japan), BET specific surface area was measured by N_2 adsorption at 77 K (TriStar 3000; Micromeritics, Norcross, GA), and morphologies were measured by scanning electron microscopy (SEM, TM-1000; Hitachi, Chila Vista, CA). A mixture of Al_2O_3 (Fluka 06285, Sigma-Aldrich, St. Louis, MO; purum p.a., sulfate <1g/kg, Ca <0.5 g/kg of undefined crystal structure, mean particle size 91 μm, BET specific surface area 3.25 m^2/g) and activated biocharcoal (Fluka 03866, Sigma-Aldrich, St. Louis, MO; carbon content 81 pct, mean particle size 19 μm, BET specific surface area 65.6 m^2/g) with a total weight of 0.5 g and a stoichiometric molar ratio (Al_2O_3/C = 1/3) was loaded in the crucible.

The sample surface temperature $T_{surface}$ was calculated based on the measured thermocouple temperature T_{TC} (Figure 5) by applying a simplified heat-transfer model. In a first step, the stagnation temperature of the crucible $T_{stagnation}$ was determined as shown in the following equation by solving the overall energy balance without a chemical reaction and a least-square fitting to

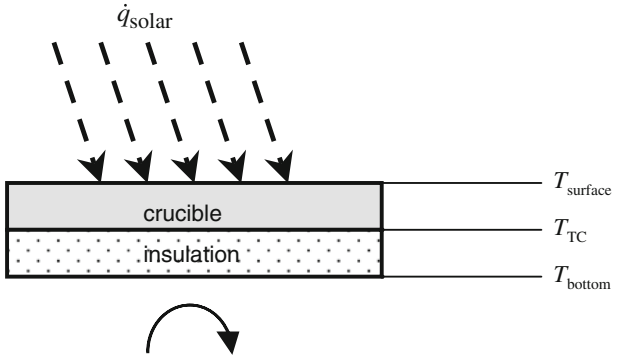

Fig. 5—1D heat transfer model through crucible and insulation.

the last 200 K of the measured heating curves (after reaction completion):

$$m \cdot c_p \cdot \frac{dT_{TC}}{dt} = \alpha \cdot \dot{q}_{solar} - \varepsilon \cdot \sigma \cdot T_{TC}^4 - k \cdot (T_{TC} - T_{ambient}) \quad [2]$$

A one-dimensional (1D) steady-state heat conduction problem then was solved across the crucible (k = 6.3 W/m K, d = 2 mm) and the insulation (k = 0.2 ± 0.1 W/m K, d = 2 ± 0.1 mm) to yield $T_{surface}$:

$$T_{surface} = T_{stagnation} + (T_{stagnation} - T_{bottom}) \times \frac{(d/k)_{crucible}}{(d/k)_{insulation}} \quad [3]$$

where the temperature outside the insulation T_{bottom} was set to 298 K (25 °C) to give an upper limit for $T_{surface}$, and the temperature gradient through the remaining sample (0.001 to 0.056 g) was neglected. The estimated error was ±50 K for $T_{stagnation}$ and was ±8 pct for $T_{surface}$. Based on comparable experiments,[24] a mean $T_{surface}$ was taken as representative during the carbothermal reduction phase.

IV. RESULTS AND DISCUSSION

Figure 6 shows the mean incident radiative heat flux onto the 24-mm-diameter target, the crucible bottom temperature, the calculated sample surface temperature, the reactor pressure, and the CO concentration in the product gas during a typical experimental run. The total pressure in the reactor was 3.5×10^{-3} bar at the beginning and was maintained between 5×10^{-3} to 12×10^{-3} bar toward the end of a run depending on the filter loading and the CO release rate. Condensed products were deposited on the upper part of the quartz tube (Figure 4). These particles had an average BET specific surface area of 17.9 m^2/g. Their XRD spectrum is shown in Figure 7, revealing the presence of only Al and Al_2O_3, the latter formed presumably by reoxidation of Al(g) with CO, either heterogeneously at the tube surface or on condensation in the aerosol. In other experimental runs, species Al_4C_3 or Al_4O_4C also

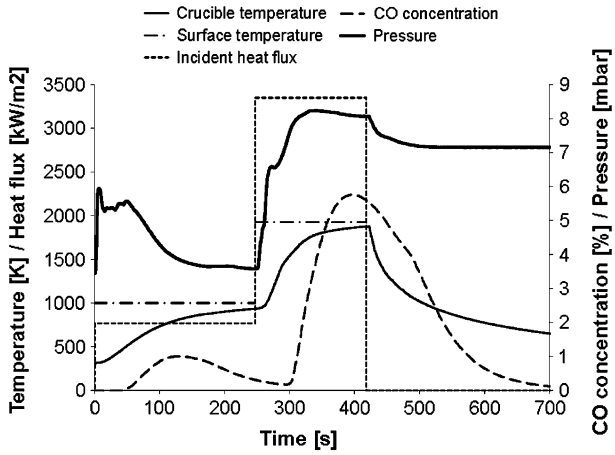

Fig. 6—Variation of the incident radiative heat flux, crucible temperature, reactor pressure, and CO product concentration during a representative solar experimental run.

were identified by XRD in the condensed deposits. The material left in the crucible contained Al_4C_3, Al_4CO_4, and nonreacted Al_2O_3 and charcoal. Note that the transparent quartz tube was maintained at below approximately 500 K (227 °C) by forced convection with the Ar flow. Thus, no reaction was expected between SiO_2 and gaseous species or solid deposits, as confirmed by inspection after the experimental runs, which revealed no signs of quartz abrasion.

A series of 14 experimental runs were performed at various radiative heat fluxes and resulting $T_{surface}$. The Al mass fraction of the products deposited in the quartz tube was determined based on the normalized reference intensity ratio of the XRD pattern, calibrated with a synthetic mixture of a known ratio of the components. The reported maximum standard deviation by this method is 8 pct.[25] Figure 8 shows the Al mass fraction of these deposits as a function of $T_{surface}$. For those runs performed at $T_{surface} > 1660$ K (1387 °C), the Al mass fraction ranged between 4 and 19 wt pct, but no temperature dependence could be elucidated. Also shown in Figure 8 is the reaction extent, defined as the ratio of the mass of CO produced and the theoretical mass of CO corresponding to complete conversion. As expected, the reaction extent increased with $T_{surface}$ and reached 55 pct at 2000 K (1727 °C). No complete conversion was possible because of the formation of by-products (Al_4C_3 and Al_4O_4C) and because of displacement of some portion of the reactants—presumable by the carrier gas—as it was found at other locations in the reactor. The increase in the bulk sample temperature (described by the crucible temperature in Figure 6) lagged behind the rapid stepwise increase in the surface temperature, which responded rapidly to the increase in the incident radiative flux. During most of the reaction period, the bulk sample was subjected to temperatures in the range 1000 K to 1700 K (727 °C to 1427 °C) and pressures in the range of 3.5 to 12 millibar. It therefore may be possible to explain the formation of free Al(g) as a result of the reaction at the hot sample

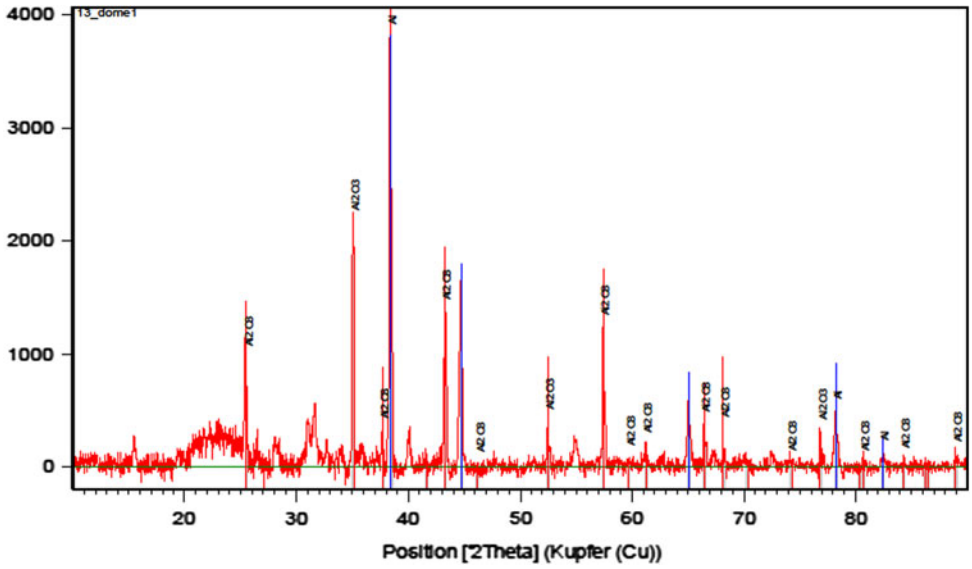

Fig. 7—XRD analysis of the quartz tube deposits.

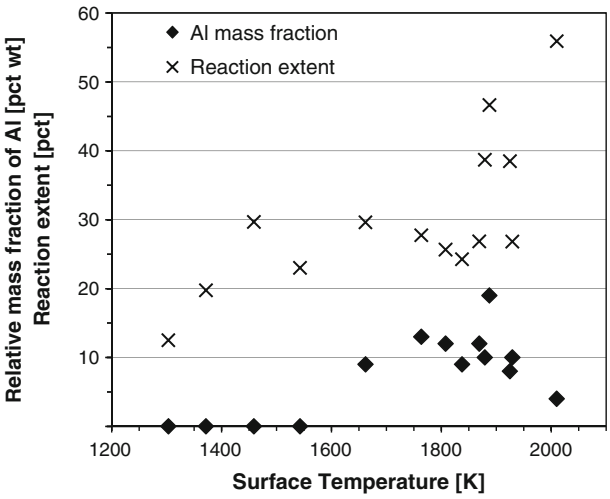

Fig. 8—Aluminum yield in the quartz tube deposits and reaction extent as a function of the calculated sample surface temperature.

surface and the formation of the by-products Al_4C_3 and Al_4O_4C as a result of the reaction in the bulk sample. These results are in agreement with the thermodynamic analysis.

Figure 9 shows the SEM of the initial Al_2O_3/charcoal mixture (Figure 9(a)), the products collected on the reactor walls (Figure 9(b)), and the products collected in the crucible (Figure 9(c)). In Figure 9(a), clearly distinguished by their size and textural characteristics are the larger, nonporous Al_2O_3 particles (left, mean particle size = 91 μm) and the smaller charcoal particles (right, mean particle size = 19 μm) that offer a larger specific surface area. In Figure 9(b), relatively large spherical-type particles were found with $d_p \approx 5$ to 10 μm. Similar morphologies were found previously in the quench zone of a ZnO dissociation reactor,[26] where their formation was explained by both condensation and coalescence of the metal vapor at short residence times in the gas phase. Besides these spheres, filamentary and rod-like structures were observed, typical for Al_2O_3 built up by Al reoxidation. In Figure 9(c), the image is dominated by rough and edged surface structures, resulting from carbide and oxycarbide formation as well as by unreacted Al_2O_3.

V. CONCLUSIONS

The vacuum carbothermal reduction of Al_2O_3 facilitates the production of Al by lowering the onset temperature for this reaction and by shifting the formation of free Al(g) to a temperature range in which the formation of Al_2O, Al_4C_3, and Al-oxycarbides is thermodynamically unfavorable. Thermodynamic equilibrium calculations predict the presence of the free Al metal in the gas phase, which can be distilled from the solid oxide. At 10^{-6} bar, Al is present at as low as 1370 K (1097 °C), suggesting the potential use of conventional reactor materials for large-scale applications. This highly endothermic reaction may be driven by high-temperature process heat supplied by concentrated solar energy, induction furnaces, or electric discharges. Using concentrated solar energy, this reaction promises significant fuel savings and CO_2 emission avoidances vis à vis the conventional Hall–Héroult electrolytic process. Carbon monoxide coproduced may be used as combustion fuel for power generation or water–gas shifted to syngas and may be processed to synthetic liquid fuels and materials. In exploratory experimental runs under concentrated thermal irradiation in Ar atmosphere, at 3.5 to 12 millibar total pressure, Al and CO were formed in the gas phase from Al_2O_3 and charcoal at temperatures as low as 1660 K (1387 °C); however, they were accompanied by Al_4C_3

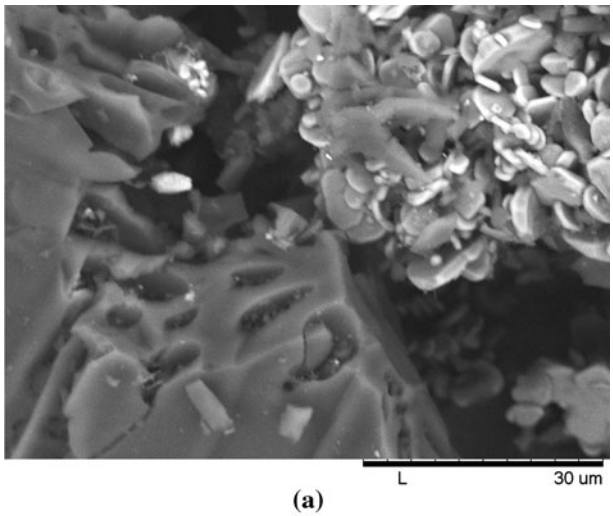

(a)

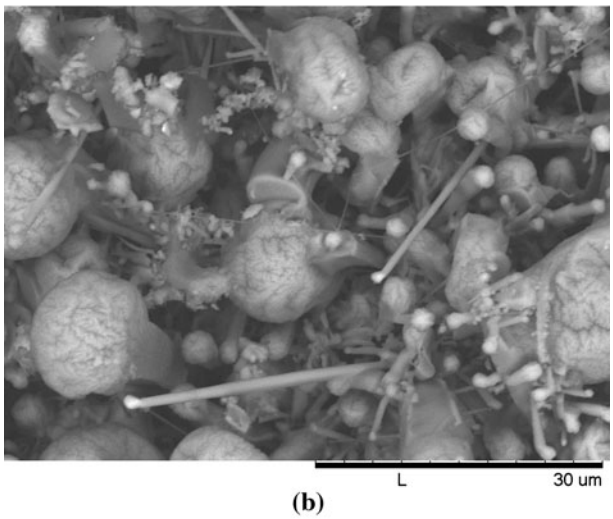

(b)

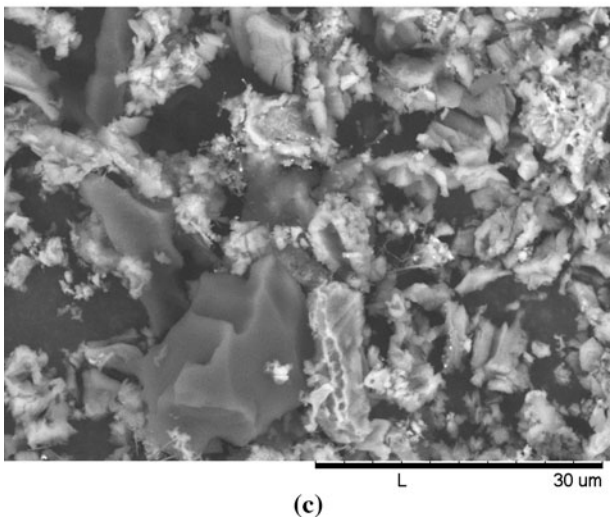

(c)

Fig. 9—SEM of (*a*) initial Al_2O_3:C mixture, (*b*) condensed products collected on the quartz tube walls, and (*c*) products collected on the crucible.

and Al_4O_4C, which is consistent with the calculated equilibrium composition at this temperature and pressure.

ACKNOWLEDGMENTS

The authors thank V. Gianini, P. Haueter, L. Schlumpf, and A. Frei for technical support with the reactor design and during the solar experimental campaign.

NOMENCLATURE

α	absorptivity
ε	emissivity
σ	Stefan–Boltzmann constant (5.6705×10^{-8} W/m^2K^4)
c_p	heat capacity (J/kg K)
d	thickness (mm)
k	thermal conductivity (W/m K)
m	mass (kg)
$\dot{q}_{solar}$	solar radiative flux (W/m^2)
t	time (s)
T	temperature (K)
TC	thermocouple
WGS	water–gas shift
ΔH	enthalpy change (kJ/mol)
ΔG	Gibbs free energy change (kJ/mol)

REFERENCES

1. International Aluminum Institute: *Aluminum for Future Generations Sustainability Update*, http://www.world-aluminium.org, 2007.
2. W.T. Choate and J.A.S. Green: U.S. *Energy Requirements for Aluminum Production, Historical Perspective, Theoretical Limits and New Opportunities*, http://www1.eere.energy.gov/industry/aluminum/pdfs/al_theoretical.pdf, 2003.
3. W. Choate and J. Green: in *Light Metals 2006 Volume 2: Aluminum Reduction Technology*, J. Galloway, ed., Wiley, New York, NY, 2006, pp. 445–50.
4. J.H. Cox and L.M. Pidgeon: *Can. J. Chem.*, 1963, vol. 41, pp. 671–83.
5. M. Halmann, A. Frei, and A. Steinfeld: *Energy*, 2007, vol. 32, pp. 2420–27.
6. T.J. Fruehan, Y. Li, and G. Cargin: *Metall. Mater. Trans. B*, 2004, vol. 35B, pp. 617–23.
7. R. Winand, M. Van Gysel, A. Fontana, L. Segers, and J.C. Carlier: *Min. Process. Extractive Metall.*, 1990, vol. 99, pp. C105–C112.
8. J.M. Toguri and L.M. Pidgeon: *Can. J. Chem.*, 1962, vol. 39, pp. 540–47.
9. J.M. Toguri and L.M. Pidgeon: *Can. J. Chem.*, 1962, vol. 40, pp. 1769–76.
10. S. Ramakrishnan and P. Koltun: *Resour. Conservat. Recycl.*, 2004, vol. 42, pp. 49–64.
11. P. Loutzenhiser, O. Tuerk, and A. Steinfeld: *J. Metals*, 2010, vol. 62, pp. 49–54.
12. A. Steinfeld: *Energy*, 1997, vol. 22, pp. 311–16.
13. J.P. Murray: *Sol. Energy*, 1999, vol. 66, pp. 133–42.
14. A. Steinfeld, P. Kuhn, and J. Karni: *Energy*, 1993, vol. 18, pp. 239–49.
15. A. Steinfeld, M. Brack, A. Meier, A. Weidenkaff, and D. Wuillemin: *Energy*, 1998, vol. 23, pp. 803–14.
16. T. Osinga, U. Frommherz, A. Steinfeld, and C. Wieckert: *J. Sol. Energ. Eng.*, 2004, vol. 126, pp. 633–37.
17. J.P. Murray, A. Steinfeld, and E.A. Fletcher: *Energy*, 1995, vol. 20, pp. 695–704.
18. J.P. Murray: *J. Sol. Energ. Eng.*, 2001, vol. 123, pp. 125–32.
19. M.E. Gálvez, A. Frei, F. Meier, and A. Steinfeld: *Ind. Eng. Chem. Res.*, 2009, vol. 48, pp. 528–33.

20. FactSage: *Thermochemical Software & Database Package*, Centre for Research in Computational Thermochemistry, Ecole Polytechnique de Montreal, Canada, www.crct.polymtl.ca, 2002.
21. National Institute of Standards and Technology: *Standard Reference Data Program*, Chemistry Webbook, http://webbook.nist.gov/chemistry.
22. A. Roine: *HSC Chemistry 5*, Outokumpu Research, Oy, Finland, 1997.
23. J. Petrasch, P. Coray, A. Meier, M. Brack, P. Haeberling, D. Wuillemin, and A. Steinfeld: *J. Sol. Energ. Eng.*, 2007, vol. 129, pp. 405–11.
24. L.O. Schunk, W. Lipiński, and A. Steinfeld: *AIChE J.*, 2009, vol. 55, pp. 1659–66.
25. F.H. Chung: *J. Appl. Cryst.*, 1975, vol. 8, pp. 17–19.
26. R. Müller and A. Steinfeld: *Chem. Eng. Sci.*, 2008, vol. 63, pp. 217–27.